An Iterative Image Dehazing Method With Polarization

Linghao Shen, Yongqiang Zhao, Qunnie Peng, Jonathan Cheung-Wai Chan, and Seong G. Kong

***Abstract*—This paper presents a joint dehazing and denoising scheme for an image taken in hazy conditions. Conventional image dehazing methods may amplify the noise depending on the distance and density of the haze. To suppress the noise and improve the dehazing performance, an imaging model is modified by adding the process of amplifying the noise in hazy conditions. This model offers depth-chromaticity compensation regularization for the transmission map and chromaticity-depth compensation regularization for dehazing the image. The proposed iterative image dehazing method with polarization uses these two joint regularization schemes and the relationship between the transmission map and dehazed image. The transmission map and irradiance image are used to promote each other. To verify the effectiveness of the algorithm, polarizing images of different scenes in different days are collected. Different algorithms are applied to the original images. Experimental results demonstrate that the proposed scheme increases visibility in extreme weather conditions without amplifying the noise.**

***Index Terms*—Dehazing, polarization, iterative scheme, weighted regularization.**

I. Introduction

IN HAZY weather conditions such as fog and mist, scene radiance can significantly be altered due to light scattering caused by dust particles in the atmosphere. Such degradation may cause poor image contrast, inauthentic color fidelity, and loss of scene details resulting in degraded object recognition capability in many visual surveillance applications [23] including urban transportation, outdoor video surveillance, and driver assistance systems [1]–[3]. There has been an increasing demand for effective measures to reduce haze effects in the acquired images.

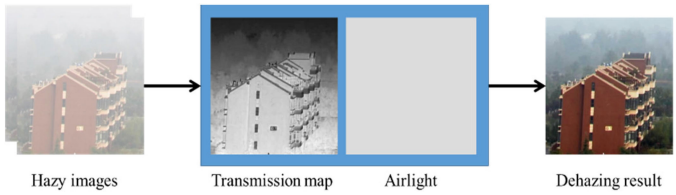

Fig. 1. Typical image dehazing process.

Image dehazing aims at reconstructing an image of high quality from its degraded version taken in hazy weather conditions. As a typical ill-posed inverse problem, image degradation process is generally modeled by

$$I(x) = L(x)t(x) + A_\infty(1 - t(x)) \tag{1}$$

where $L(x)$ denotes the radiance of a haze-free scene on a clear day at a spatial location x, A_∞ is the intensity of the airlight at infinity. $I(x)$ denotes the degraded version of $L(x)$ by atmospheric scattering. Transmission map $t(x)$ represents the rate of transmission, describing the scattering and absorption of radiance through particulates in the atmosphere. $L(x)$ can be calculated by

$$L(x) = \frac{I(x) - A_\infty(1 - t(x))}{t(x)}. \tag{2}$$

The key point of image dehazing is to estimate the $t(x)$ and A_∞. A_∞ is the scene unrelated parameter which can be estimated by a pre-processing step. eq. (2) can be simplified as a transmission map estimation problem. Fig. 1 shows a typical image dehazing process.

Existing methods for estimation of transmission map can be based on single image or multiple images. In single image based methods, some image statistical priors like local contrast [1], dark channel [3], non-local [5] are used to regularize the transmission map estimation. As for multiple images based methods, atmospheric optical features such as polarization [10] are used to regularize the transmission map estimation process.

Tan [1] used both the chromaticity and value of infinite sky to get the transmission map. The dehazing results are found to be not satisfactory with some halos. Fattal [2] described a single image method to obtain solutions where surface shading and transmission function are locally uncorrelated. However, this method fails when the image has a low SNR value. He *et al.*

Manuscript received January 11, 2018; revised April 30, 2018, July 18, 2018, and September 2, 2018; accepted September 4, 2018. Date of publication September 24, 2018; date of current version April 23, 2019. This work was supported in part by the National Natural Science Foundation of China (61771391, 61371152); in part by the Shenzhen Municipal Science and Technology Innovation Committee (JCYJ20170815162956949); in part by the National Natural Science Foundation of China and Korea National Research Foundation Joint Funded Cooperation Program (61511140292, NRF-2015K2A2A2000886); and in part by the Korea National Research Foundation (NRF-2016R1D1A 1B01008522). The associate editor coordinating the review of this manuscript and approving it for publication was Prof. Zixiang Xiong. *(Corresponding author: Yongqiang Zhao.)*

L. Shen and Y. Zhao are with the School of Automation, Northwestern Polytechnical University, Xi'an 710072, China (e-mail: 460855258@qq.com; zhaoyq@nwpu.edu.cn).

Q. Peng is with the Luoyang Institute of Electro-optical Equipment of AVIC, Luoyang 471000, China (e-mail: pengqn1992@126.com).

J. C.-W. Chan is with the Department of Electronics and Informatics, Vrije Universiteit Brussel, 1050 Brussels, Belgium (e-mail: jcheungw@etrovub.be).

S. G. Kong is with the Department of Computer Engineering, Sejong University, Seoul 05006, Korea (e-mail: skong@sejong.edu).

Color versions of one or more of the figures in this paper are available online at http://ieeexplore.ieee.org.

Digital Object Identifier 10.1109/TMM.2018.2871955

[3] found that the values of a color channel of clear images are always very small. Using this observation as prior, the transmission of fog is estimated. Many dehazing researches based on He's dark channel prior were developed for the advance of the dehazing algorithms [20]. Based on the strong recurrence property that small image patches can be repeated at different scales in natural images, Bahat and Irani [4] exploited the deviation from ideal patch reoccurrence in the estimation of local airlight and relative transmission at different distances. Berman *et al*. [5] utilized the non-local prior, computing the distribution of values of all color channels which built the hazy-lines. Transmission and airlight can be estimated with hazy-lines. Codruta *et al*. [21] used the information existing in the single input image for multi-scale fusion-based dehazing. By assuming that a linear relationship exists in the minimum channel between the hazy image and the haze-free image, Wang *et al*. [25] estimated transmission map which is used for dehazing. Fan *et al*. [29] use two-layer Gaussian process regression (GPR) to learn the relationship between the hazy image and the transmission map, and smooth the final transmission map with local information. To estimate the scene transmission, Ren *et al*. [27] use a coarse-scale network to obtain the transmission map and then refine it using a fine-scale network. Using a learned model, Tang *et al*. [6] added more features for foggy images based on the dark channel prior to achieve successful dehazing in certain weather conditions. Song *et al*. [26] used Ranking Convolutional Neural Network to learn powerful haze-relevant features which are used for dehazing. Cai *et al*. [7] use a deep learning approach with DehazeNet for transmission estimation. The input layers contain almost all haze-relevant features and a novel nonlinear activation function is used to improve the final result. Zhu *et al.* [30] combine generative adversarial network (GAN) and usual dehazing process, getting the clear image and intermediate parameters at the same time. Li *et al.* [31] use convolutional neural network to reconstruct the clear image directly from the hazy image, without calculating the intermediate factors. These methods above are effective in light hazy condition. However, estimating the transmission map is challenging for a given image taken in heavy hazy conditions. In heavy haze conditions, visual information loses quickly, so restoring a clear image becomes hard by previous methods.

In hazy weather, scattering will be propagated and the atmosphere light becomes stronger and polarized. Using the polarization properties of the light, scattered light can be removed effectively with a polarizer. The polarization information can also be utilized as a prior to regularize the transmission map estimation. Schechner *et al*. [10] used polarized images to estimate the transmission map. Shwartz *et al*. [11] proposed a mathematical method using Independent Component Analysis to isolate the airlight from the reflected light, then accurate transmission map is obtained with the estimated airlight. Without including any sky region, Miyazaki *et al*. [12] used the polarization information of similar objects at different distances to estimate the polarization factors. While the result is reasonably accurate, objects at different distances may not appear in the polarized images. Liang *et al*. [13] used polarization angles to estimate factors such as the degree of polarization of airlight (DPA). They found that visual improvement was achieved especially in extreme weather. With a similar approach, Qu *et al*. [14] used the brightest pixels of both the intensity image and the polarization difference to estimate the airlight. And DPA is calculated based on the dependency between DPA and airlight.

Existing dehazing methods can improve visibility, but noise will become more serious with increasing hazy level. The noise is associated with the transmission map, and the accuracy of the latter depends on the density of haze and the distance between the scene and the imaging device. Therefore, denoising after dehazing may end up with two scenarios: the noise will not be suppressed or the image details can be destroyed. As the distance and the degree of the haze density increase, the value of the transmission map would increase exponentially. As a result, the noise becomes so overwhelming that image quality becomes very low. In addition, the noise actually varies at different locations and it depends on the transmission map. As traditional denoising methods have a local consistency, they are not effective.

For most scenes, the depth and chromaticity information in local regions is rather consistent. A transmission map can provide local depth information as well as information pertaining to noise amplification and these could be used as a guide for denoising. An irradiance image with chromaticity information can also be used as a guide for denoising. An accurate transmission map using irradiance as feedback could suppress the noise. At the same time, as transmission map is estimated from irradiance, a more accurate transmission map can be acquired by a clearer irradiance image. The quality of transmission map and irradiance image can promote each other. First, local depth consistent prior is used as the guide information to improve the quality of transmission map. Then optimized transmission map is used to improve the quality of the irradiance image. Based on the coupled relationship between transmission map and irradiance image, an iterative image dehazing method is proposed in this paper.

The main contributions of this paper include:

1) An imaging model to consider both the noise and the noise amplified during the dehazing process is proposed.
2) Based on the depth and chromaticity information correlation in local regions, a joint depth-chromaticity regularization and a joint chromaticity-depth regularization are proposed for transmission map and dehazed image denoising.
3) An iterative scheme combining the weighted regularization to substantially improves the quality of dehazing.

The rest of this paper is organized as follows. Section II presents the basic knowledge of polarization dehazing. Section III presents the targeted problem. Then an iterative scheme for joint optimization method is proposed in Section IV. Finally, we show the experimental results in Section IV and conclude this paper in Section V.

The Matlab source code and the data is available online at https://github.com/polwork.

II. Image Dehazing

To derive the scene radiance, $t(x)$ should be acquired. The transmission map $t(x)$, $0<t(x)<1$, can be expressed as an

exponential function of the distance [1]:

$$t(x) = \exp\left(-\beta z(x)\right) \tag{3}$$

where β denotes the optical density of the particles in the atmosphere, which is assumed to be a constant at any specific wavelengths. The depth map $z(x)$ indicates the distance from the camera to a scene point at a spatial location, x, in the image.

For an outdoor haze-free image L, except for the sky region, some dark pixels with very low intensity exist in at least one of the color (RGB) channels [3]. As the intensity of dark pixels tends to be zero, it is called dark channel prior. While for a hazy image, the intensity of these dark pixels in that channel is mainly contributed by airlight A. Based on this prior, $t(x)$ can be estimated as [3]:

$$t = 1 - w \min_{y\in\Omega(x)}\left[\min_{c}\frac{I_c(y)}{A^c}\right] \tag{4}$$

where ω is a constant parameter, $\Omega(x)$ is a local patch centered at x, and $c\ \epsilon\{\mathrm{R, G, B}\}$ is the color channel index.

Forced by strong polarization effects of the suspended particulates as a result of backward scattering, the airlight A is a partially polarized light. But because of the depolarization effect of the suspended particulates, the irradiance reflected from the scene through the haze (D) could be treated as unpolarized light as compared to the airlight. Based on the polarized scattering effects, t can be estimated as:

$$t = 1 - \frac{(I^{\perp} - I^{//})A}{A_{\infty}(A^{\perp} - A^{//})} \tag{5}$$

where $I^{//}$ and $I^{\perp}$ are images acquired through polarizers at 0° and 90°, respectively.

The quality of the restored image is closely related with the estimation of $t(x)$. To evaluate the performance of single image dehazing method and polarization dehazing method, we set up a hazy image database of 1000 images taken in different hazy weather conditions. Some examples of these images are shown in Fig. 2. FADE [17] is calculated to represent the visibility after dehazing. A lower FADE value means a clearer condition and higher visibility. We applied three typical dehazing methods: dark channel method [3], Non-local based method [4] and polarization based method [10], to small foggy patches and FADE values of the dehazed patches are presented to represent degree of clearness. Fig. 3 shows FADE as a function of dark channel value for different dehazing methods. A large dark channel value means that the image is brighter, which can be considered a hazier situation. Dark channel value is represented by the largest value in the dark channel [3]. Based on dark channel value of image, hazy images are grouped into two sets roughly, light haze (dark channel value lower 150) and heavy haze (dark channel value higher than 150). The performance of the dark channel method, non-local based method and polarization based method were similar in cases with low haze density. However, as the haze density increases, the dark channel and non-local based methods' performance drops quickly. In contrast, the polarization method maintains consistently outstanding performances even in extremely hazy conditions, better than the dark channel and non-local based methods. It can be concluded that polarization based dehazing method has relative stable dehazing performance even in heavy hazy weather condition. In this paper, we will focus on improving the performance of polarization dehazing method.

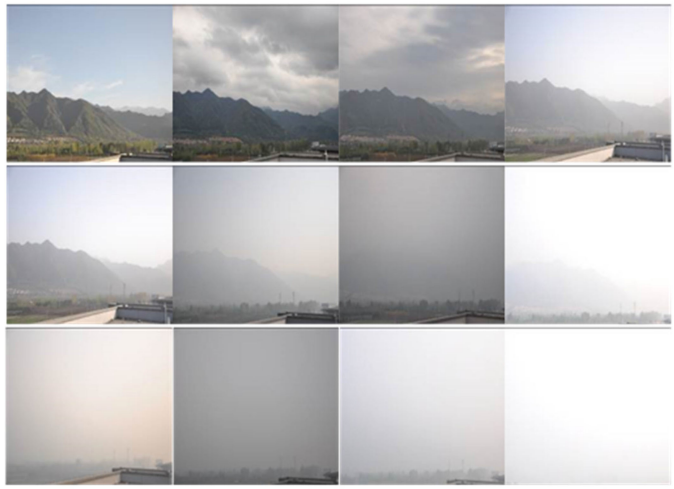

Fig. 2. Images of the same scene taken under different haze conditions, from clear day to extremely hazy weather.

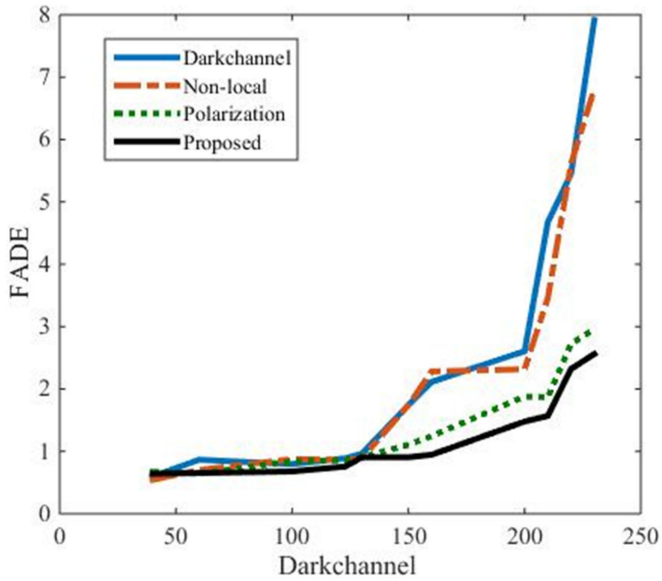

Fig. 3. FADE [17] is an evaluation value dehazing methods based on dark channel [3], non-local [5], Polarization [10] and proposed method. A higher value means a heavier haze.

III. Problem Definition

Most existing image dehazing methods are based on imaging models without accounting for imaging noise. In actual situations, however, any acquired image is corrupted by noise to a certain extent. This noise is mainly caused by optical imaging sensor due to the level of illumination and the electronic circuits, and image noise can be modeled by additive noise model [22]. Taking the additive noise into consideration, the image

Fig. 4. The upper row shows (a) Hazy image, (b) Dehazing result with polarization, (c) Dehazing result with dark channel. The bottom row is a zoom in of the sky region to show noisy effect after dehazing.

Fig. 5. Dehazing results of scenes in different haze conditions with polarization. The dehazing performance decreases with more noise and artifacts as haze density increases.

degradation model is given by

$$I = L_0 t + A_\infty (1 - t) + n \tag{6}$$

where n denotes the imaging noise, L_0 is still the initial irradiance of the scene. From (6), L_0 can be expressed as

$$L_0 = \frac{I - A_\infty (1 - t)}{t} + \frac{n}{t}. \tag{7}$$

Compared with (2), after dehazing, L_0 can be represented by

$$L_0 = L + \frac{n}{t}. \tag{8}$$

Eq. (8) shows that the recovery result is the original irradiance mixed with added noise divided by t. The transmission t ranges between 0 and 1 meaning that the added noise can be amplified.

Fig. 4 shows that some noise and artifacts become more visible after dehazing, especially in the sky region using the methods based on polarization and dark channel. From (8), the final irradiance of the scene has been mixed with the noise n. The added noise ε is given by

$$\varepsilon = \frac{n}{t} = n \exp(\beta z). \tag{9}$$

Eq. (9) shows that the noise becomes serious as the fog density and the depth of the scene increase. If β (or z) is fixed, the noise would increase exponentially as z (or β) grows.

A. Factor β

From the analysis above, we have learnt that the degree of noise is positively related to the degree of haze. To further illustrate this is real, we collected images in different weather conditions and applied the polarization dehazing method described in [9]. We collected 300 images of a red brick house in different weather conditions. Fig. 5 shows dehazing effects of low density (b and c) and high fog density (e and f). After polarization dehazing, the image quality generally improves, but at the same time, the noise effect becomes more serious as fog density increases (Fig. 5(e) and 5(f)).

To analyze the noise level in dehazed image with different haze levels, we compare the deviation (or absolute difference) between each pixel and the image mean in the same region acquired at low and high haze levels. The histograms in Fig. 6 show that deviations are higher in heavy-haze patch indicating higher level of noise. And as shown in (9), the noise would increase as β grows.

B. Factor z

As the distance between the scene and imaging device increases, the dehazing result will be affected by more noise and artifacts. Fig. 7 compares the dehazing results of far and near objects. The dehazing result of objects like building in various distances show that noise issue with distant objects is bigger. Two objects, one far at region 2 and one near at region 1, both with smooth surface are selected from an image which has been dehazed (Fig. 7). The far object has a larger deviation as illustrated in Fig. 7 and explained by (9). As the density of haze or the distance of the objects increases, the negative impact of the atmosphere becomes more serious. As a result, the value of the transmission map decreased rapidly, even approaching zero. These effects ultimately result in amplified noise and image distortion. Near objects however are less influenced by the noise. Thus the noise that is amplified after dehazing is not globally consistent, and this can explain why results from existing

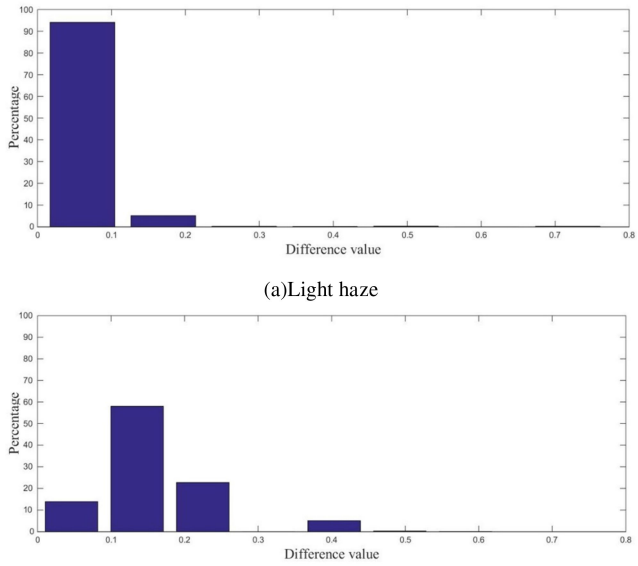

Fig. 6. Distributions of the deviation from the mean value of the low-haze patch Fig. 5(c) (TOP) and high-haze patch Fig. 5(f) (BOTTOM). Horizontal axis is the absolute difference from mean, and vertical axis is the percentage frequency.

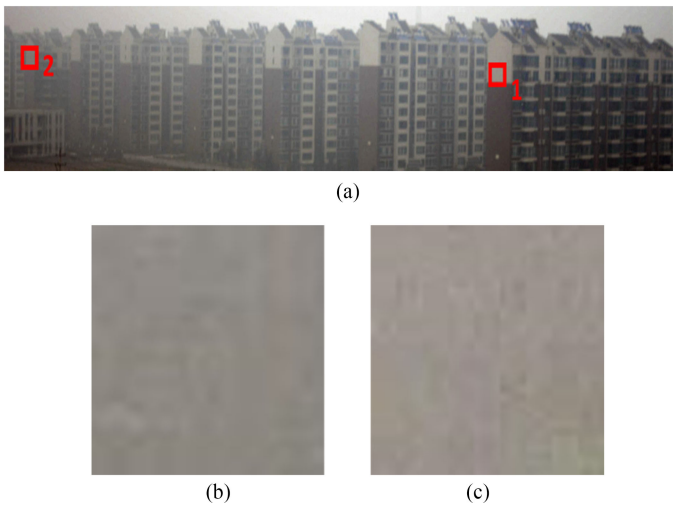

Fig. 7. (a) Dehazed image by polarization, (b) Zoomed far object 2, (c) Zoomed near object 1.

denoising methods which can be used after dehazing are not satisfactory.

To analyze the noise level in dehazed image with different distance, we compare the deviation (absolute difference from image mean) of dehazed patches at different distances. Fig. 8 shows the distribution of deviation for Fig. 7(b) and (c). The horizontal ordinate presents the absolute difference between the pixel value and the mean value of the patch, and the vertical ordinate represents the distribution of the differenced values. Comparing Fig. 8(a) and (b), there are much less percentage of small values in the far scene than in the near scene. This indicates that the noise content of the far scene is much higher and that the noise increases with the increase of depth.

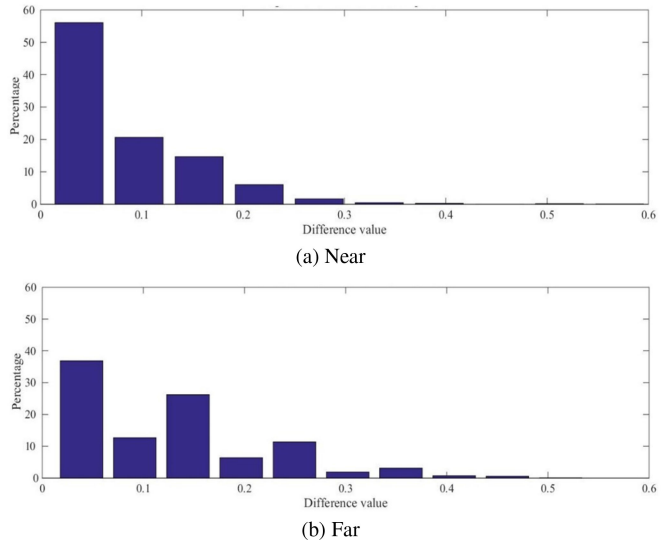

Fig. 8. (a) Histogram of deviation from the mean of the patch Fig. 7(c) and (b) is the same from Fig. 7(b).

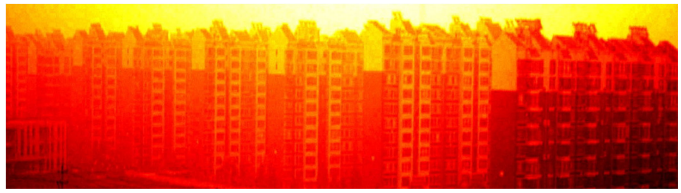

Fig. 9. 2D image representation of the βz term denoting relative depth map.

C. Depth Map

Through the experiments and the statistical result above, the variance of the smooth area increases as the distance or the haze degree increases. The noise has a positive correlation with the distance and the degree of the haze, which coincide with the result from theoretical derivations, βz is associated with the noise. Eq. (3) shows that the transmission map is a function of the distance and fog density. From (9), when the noise n is constant, the added noise ε is inversely proportional to the value of the transmission map. From (3) and (9), βz is given by

$$\beta z = -\ln(t) \tag{10}$$

Fig. 9 shows the depth map (βz) calculated from the image in Fig. 7(a). The value of βz is associated with the distance between the object and the image acquisition equipment. Supposing that the density of the fog (β) is instant in a short time, the image of βz shows the relative depth of the scene. The larger the values of βz (lighter in the image), the higher the noise level. This observation suggests that it is possible to deal with the noise after dehazing with the help of the transmission map.

The proposed idea is to improve image quality by denoising an image which has been dehazed, or a dehazed image. We applied BM3D [16], a popular image denoising method, to enhance a dehazed image and the result is shown in Fig. 10. Fig. 10(a) is a dehazed image and Fig. 10(b) is after denoising method BM3D has been applied. With the enlarged images, we can see the near objects like wires are sharper, but far objects like the

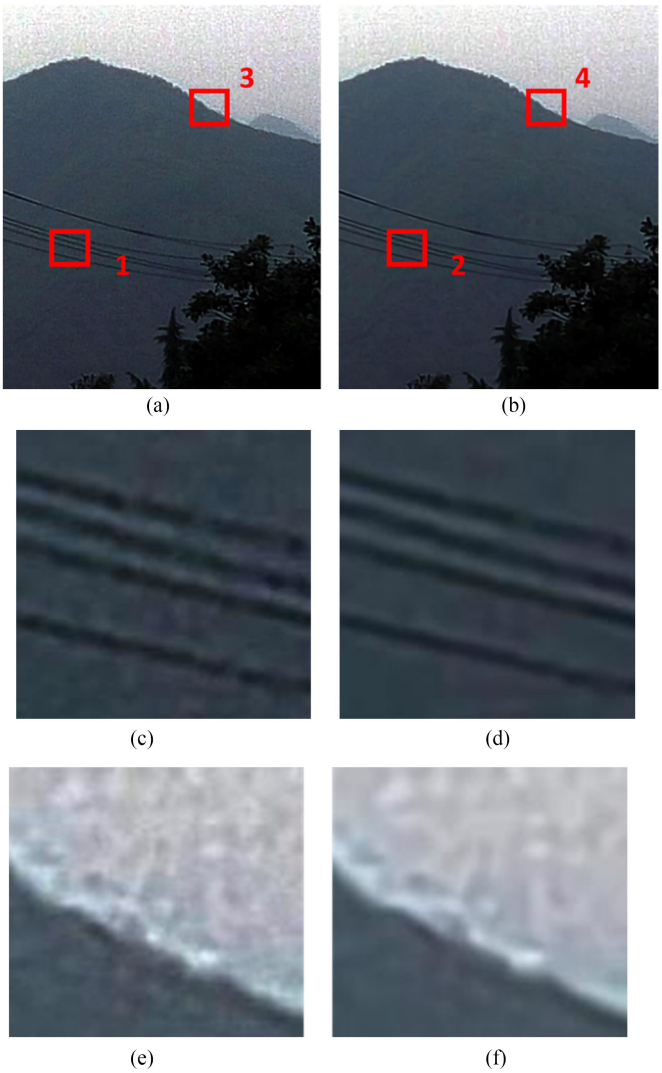

Fig. 10. Dehazing result shows a high level of noise in the whole image especially in the sky region and the denoising: (a) Dehazing result, (b) Dehazing after denoising by BM3D, (c), (d), (e), (f) are the zoom images of regions 1,2,3,4, in (a) and (b).

sky has little improvement and the sky regions are still covered with noise. To achieve the goal of dehazing the images acquired with different haze levels with objects in various distances, the core issues are: (a) local distortion according to fog density and (b) the distance between the objects and the image acquisition equipment.

IV. An Iterative Scheme for Joint Optimization

In conventional dehazing approaches, visibility enhancement and noise suppression are treated separately. Such scheme suffers from distortions and excess smoothness. Visibility enhancement often leads to amplification of non-local noise. Since visibility enhancement and noise are correlated, it is logical to incorporate visibility enhancement in denoising. But denoising without considering the local consistency will erase details [24] and is not suitable for the dehazing progress. As the transmission map keeps local consistency, an iterative scheme using information from a transmission can improve the final dehazing result.

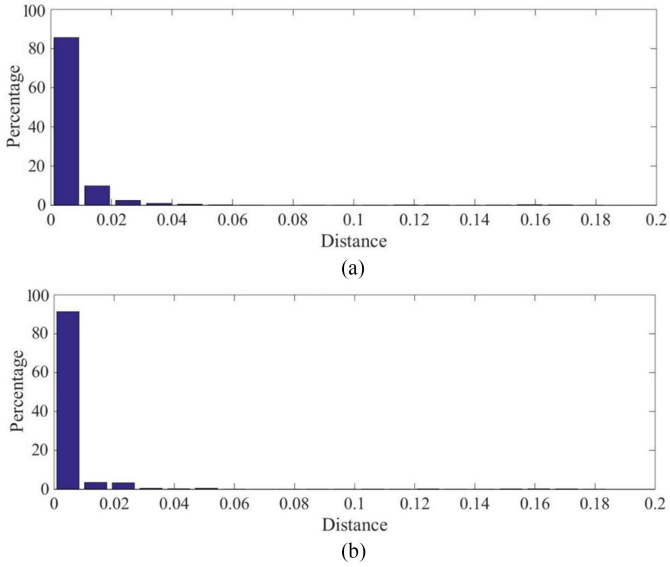

Fig. 11. (a) Depth distance histogram, (b) Chromaticity distance histogram where depth distance < 0.05.

A. Joint Depth-Chromaticity Compensation Regularization for Transmission Map

For a transmission map, depth and spatial information of a local neighborhood are highly correlated. Depth distance in transmission map and chromaticity distance (in a dehazed image) between two pixels x and y is defined as:

$$D_1(x,y) = |z(x) - z(y)| \tag{11}$$

$$D_2(x,y) = |C_L(x) - C_L(y)| \tag{12}$$

where $z(x)$ and $z(y)$ denote depth information at pixel x and y respectively and $C_L(x)$ and $C_L(y)$ denotes color channel intensity at pixel x and y of a haze free image respectively ($z(x)$, $z(y)$, $C_L(x)$ and $C_L(y)$ are normalized values between 0 and 1). To use D_1 and D_2 for further analysis, 100 haze free images and corresponding depth maps are collected. A 5×5 window is run where the absolute difference between the middle pixel x and all 24 neighborhood pixels (y) are calculated. For an image with size m by n, a total of $(m-2)(n-2)^*24$ D_1 or D_2 values are generated. The D_1 and D_2 values from 100 images are lumped together to show their distributions.

Fig. 11 show the depth distance and chromaticity distance from 100 depth maps and corresponding haze free images. In the depth distance histogram (Fig. 11(a)), approximately 90% of the pixels have depth distance smaller than 0.05. For most natural images, depth is highly correlated among local neighborhood pixels. And for regions with high depth correlations, the chromaticity is also highly correlated in dehazing results as shown in Fig. 11(b).

Estimated transmission map must retain high depth correlation besides edge region, and estimated dehazing results must retain high chromaticity correlation in transmission map

correspond region. To ensure edge, depth and chromaticity consistency in the estimated transmission map and dehazing results, a joint depth-chromaticity compensation regularization is defined as:

$$E_1(t,L) = \sum_x \sum_{y\in\Omega(x)} W_1(x,y)\|t(x) - t(y)\|_2 \tag{13}$$

$$W_1(x,y) = \frac{1}{2\sigma^2}\exp\left(-\sum_{i\in R,G,B}\|L(x) - L(y)\|_2^2\right) \tag{14}$$

where $W(x,y)$ is the weight function, i denotes color channels, $t(x)$ and $t(y)$ denote the value in the transmission map, x and y denote the spatial coordinate of pixel x and pixel y respectively, σ is the standard deviation. In the local region of the transmission map, due to the influence of noise, if the transmission difference of two pixels is large, which is often the case at the edge of regions, the color of the two pixels of the corresponding dehazed image also differs significantly, then $W_1 \approx 0$. Therefore, this paper proposes a weighted regularization term to effectively suppress the noise amplification and preserve the edge details of the transmission map. The denoised transmission map t can be estimated by:

$$t = \underset{t}{\operatorname{argmin}}\,\|t(x) - t_0(x)\|_2^2 + \lambda E_1(t,L) \tag{15}$$

where the initial estimated transmission map value is t_0, λ is the standard Lagrangian multiplier. eq. (15) can be solved by standard gradient descent method.

B. Joint Chromaticity-Depth Compensation Regularization for Dehazed Image

For clear images, depth and spatial information of a local neighborhood are highly correlated. To confirm this, we selected and analyzed statistically 100 depth maps and corresponding haze free images.

Fig. 12 is generated using the same procedure as described in the last section. It can be seen that when the depth distance is less than 0.05, the chromaticity distance which is less than 0.02 is more than 90%. This shows that, for most natural images, there is a larger color correlation consistency with depth in the local area of the scene. Estimated irradiance L must retain high depth correlation besides edge region, and estimated intensity image must retain high chromaticity correlation. To ensure edge, depth and chromaticity consistency in the estimated irradiance, a joint chromaticity-depth compensation regularization is defined as:

$$E_2(L,t) = \sum_x \sum_{y\in\Omega(x)} W_2(x,y)\|L(x) - L(y)\|_2 \tag{16}$$

where

$$W_2(x,y) = \frac{1}{2\sigma^2}\exp\left(-\sum_{i\in R,G,B}\|t(x) - t(y)\|_2^2\right). \tag{17}$$

If the chromaticity difference of two pixels is large, which is often the case at the edge of regions, the depth of the two pixels of the corresponding transmission map also differs significantly,

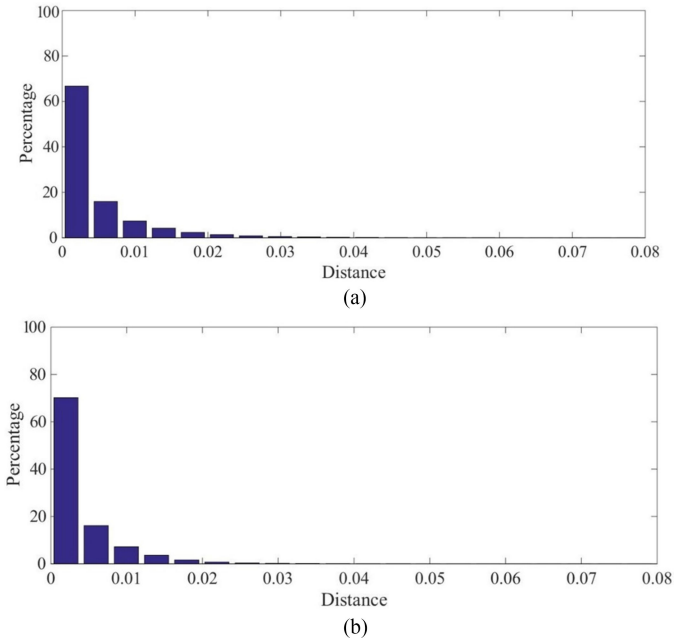

Fig. 12. (a) Chromaticity distance histogram. (b) Chromaticity distance histogram where depth distance < 0.05.

then $W_2 \approx 0$. Therefore, this paper proposes a weighted regularization term to effectively suppress the noise amplification and preserve the edge details of the irradiance. The denoised dehazed image L can be estimated by:

$$L = \underset{L}{\operatorname{argmin}}\,\|L(x) - L_0(x)\|_2^2 + \beta E_2(L,t) \tag{18}$$

where the initial value is L_0, β is the standard Lagrangian multiplier. Eq. (18) can be solved by standard gradient descent method.

C. An iterative Image Dehazing Method With Polarization

By using the previous method, noise in the calculated transmission map and irradiance image can be reduced greatly. A less noisy transmission map can enhance the quality of irradiance image, and a less noisy irradiance image can promote the performance of the joint depth-chromaticity compensation regularization algorithm for transmission map. In other words, the performance of transmission map and irradiance image is mutually beneficial. Thus, an iterative scheme is applied to solve the problem that $t(x)$ and $L(x)$ are optimized at the same time.

From the two acquired polarized image, the initial transmission map can be calculated as:

$$t_0 = 1 - \frac{(I^{\perp} - I^{//})A}{A_{\infty}(A^{\perp} - A^{//})}. \tag{19}$$

And the initial irradiance also can be calculated:

$$L_0 = \frac{(I^{\perp} + I^{//}) - A_{\infty}(1 - t_0)}{t_0}. \tag{20}$$

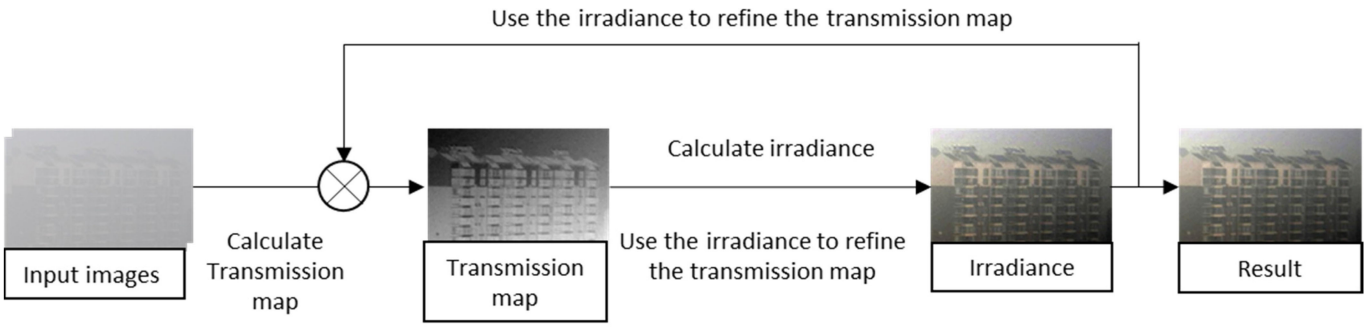

Fig. 13. Procedure of the haze removal algorithm.

So the iterative process can be written as:

$$t_{i+1} = \underset{t_{i+1}}{\operatorname{argmin}} \|t_{i+1}(x) - t_i(x)\|_2^2 + \lambda E_1(t_{i+1}, L_i) \quad (21)$$

$$L_i' = \frac{(I^{\perp} + I^{//}) - A_{\infty}(1 - t_{i+1})}{t_{i+1}} \quad (22)$$

$$L_{i+1} = \underset{L_{i+1}}{\operatorname{argmin}} \|L_{i+1}(x) - L'_i(x)\|_2^2 + \beta E_2(L_{i+1}) \quad (23)$$

where *L'* is the intermediate result of irradiance, *i* means the *i*th iteration.

The iterative process will stop when $||t_i(x) - t_{i-1}(x)|| < \varepsilon$. It has been shown typically 3 to 4 iterations are suffice for convergence. At each iteration, the noise of transmission map and irradiance decreases and the accuracy improves. And the algorithm is shown as follows:

Algorithm 1: Iterative Image Dehazing Method with Polarization

Require: $\{I_0, I_{90}\}$ (Two polarized images of 0 and 90 degrees) and *A* (estimated airlight)
Output: L_{opt} (The optimized radiance of the scene)
1: Calculate the transmission map $t_0(x)$ by EQ (19);
2: Calculate the intermediate radiance $L_0(x)$ by EQ (20);
3: **do** i = 0
Calculate the transmission map $t_{i+1}(x)$ by EQ (21);
Calculate the intermediate radiance $L_{i+1}(x)$ by EQ (23);
$i = i + 1$;
until $||t_i(x) - t_{i-1}(x)|| < \varepsilon$
4. **return** $L_{opt} = L_i$

D. Algorithm Solution

Because the solution of (21) and the solution of (23) use the same method, we will discuss only once the solving process of (21).

Then we set

$$\begin{aligned} F &= \|t_{i+1}(x) - t_i(x)\|_2^2 + \lambda E_1(t_{i+1}, L_i) \\ &= \|t_{i+1}(x) - t_i(x)\|_2^2 \\ &\quad + \lambda \sum_x \sum_{y \in \Omega(x)} W_1(x,y) \|t_{i+1}(x) - t_{i+1}(y)\|_2. \end{aligned} \quad (24)$$

Because when we optimize the transmission map t_{i+1}, we think that L_i is known. So W_1(x,y) is known and is constant in the process of optimization. The derivation of *F* is shown as follows:

$$\begin{aligned} \frac{\partial F}{\partial t_{i+1}} &= 2[t_{i+1}(x) - t_i(x)]^T \, [t_{i+1}(x) - t_i(x)] \\ &\quad + \lambda \sum_x \sum_{y \in \Omega(x)} W_1(x,y) \frac{[t_{i+1}(x) - t_i(y)]^T}{\|t_{i+1}(x) - t_i(y)\|}. \end{aligned} \quad (25)$$

In this step, we assume t_i(y) is known, and its value is the output from the last iteration. From the above equation of the derivation we can see *F* is derivable everywhere, so we can use the gradient descent method with *t* updated as follows:

$$t_{i+1} = t_i - \eta \frac{\partial F}{\partial t} \quad (26)$$

where t_i and t_{i+1} represent the values of *t* in the adjacent iterative process. η represents the step length of the iteration. Along the fastest gradient reduction direction, it is more likely to find the minimum value of the function. It is understood that the final point of gradient descent could be a local minimum instead of a global minimum point.

E. Test Data Preparation

The raw images are taken mostly in Xi'an, Shaanxi Province, China. The used digital camera is Nikon D90 mounted by a rotating polarizer. The output image size is 4288 × 2848 pixels, and its format is JPEG. The chosen scenes include buildings, statues, mountains, trees, cars, road, and so on. The distance ranges from 50 to 5000 meters. The date set contains over 300 different scenes. We took images in 400 different hazy days in recent 5 years. The haze level ranges from 40 to 245 in dark channel value, like images shown in Fig. 2. For each scene in any different day, two images are captured with the linear polarizer at the angles of 0° and 90° at the same time.

Figs. 14–20 show some examples of comparison between popular methods and our proposed method. In this paper, the parameter λ in (21) is set as 1 and the parameter β in (23) is set as 2. In the process of dehazing, transmission map and irradiance have the comparable levels of noise. If transmission map has a lower level of noise, transmission should be more dominant to reduce the influence of the noise of the irradiance. To such end, λ should be smaller than β. If the irradiance has a lower noise

Fig. 14. Dehazing results for images in different days.

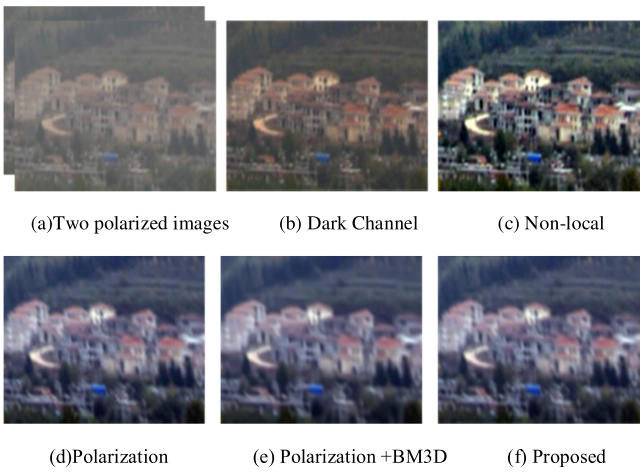

Fig. 15. Dehazing results for light-haze images.

level, then β should be smaller than λ. Based on experience, β and λ are set between 1 and 2. To get A_∞, we use the mean value of the brightest pixels.

Our results were compared with polarization based method [10], dark channel based method [3], and non-local based method [4] for images taken in light-haze and heavy-haze conditions. To evaluate the denoising after dehazing, we compare our method with the results of applying BM3D [16] to dehazed image obtained by the polarization based method.

In this paper, we collected hazy images in different days. Fig. 14 shows one of the collected scenes with increasing haze and the dehazing results of different methods. When haze is light, dark channel based method performs better in terms of visibility. And as haze increases, its quality drops sharply.

F. Dehazing Results in Different Haze Level

In a light-haze day, visibility is slightly degraded by the haze, and polarized images from two angles 0° and 90° are used, as shown in Figs. 15–17. All five dehazing methods including Polarization [10], Polarization+BM3D [16], Dark Channel [3], Non-local [5] and the proposed method, perform well to improve visibility. Dark Channel and Polarization results show problem of noise in the smooth regions. The proposed method effectively improves the contrast and reduces the noise at the same time. The polarization dehazing method followed by denoising with BM3D also have a good dehazing result, but lose some image details. It is illustrative especially in Fig. 16(e) that the house number '8' was degenerated to 'H'.

When haze is heavy, the quality of the images drops substantially. In Fig. 18 and Fig. 19, it is shown that the polarization method outperforms the dark channel and non-local based methods in extremely hazy conditions. The proposed method effectively improves the contrast without sacrificing much information of the texture and the edges. The sky has clear color distortion, and even the BM3D method could not mitigate this

(a) Original scene (b) Dark Channel (c) Non-local (d) Polarization (e) Polarization+BM3D (f) Proposed

Fig. 16. Dehazing results for light-haze images and zoom images of the red square.

(a) Original scene (b) Dark Channel (c) Non-local (d) Polarization (e) Polarization+BM3D (f) Proposed

Fig. 17. Dehazing results for light-haze images and zoom images of the red square.

(a) Original scene (b) Dark Channel (c) Non-local (d) Polarization (e) Polarization+BM3D (f) Proposed

Fig. 18. Dehazing results for heavy-haze images and zoom images of the red square.

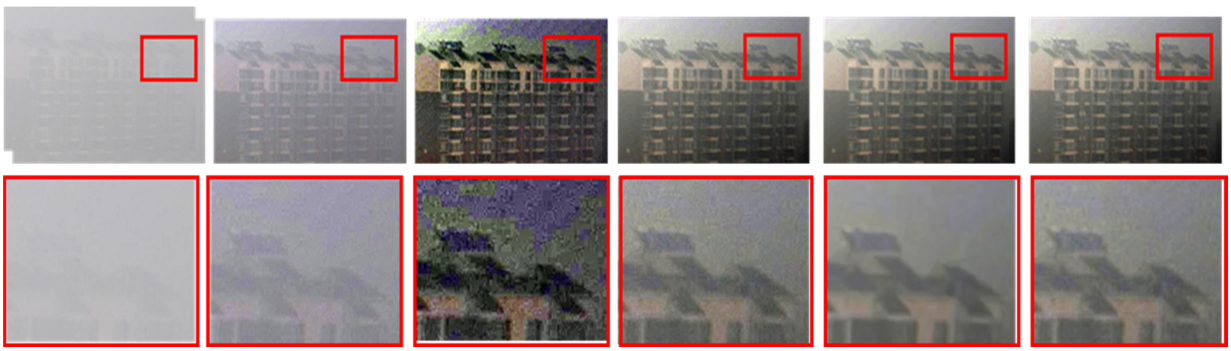

(a) Original scene (b) Dark Channel (c) Non-local (d) Polarization (e) Polarization+BM3D (f) Proposed

Fig. 19. Dehazing results for heavy-haze images and zoom images of the red square.

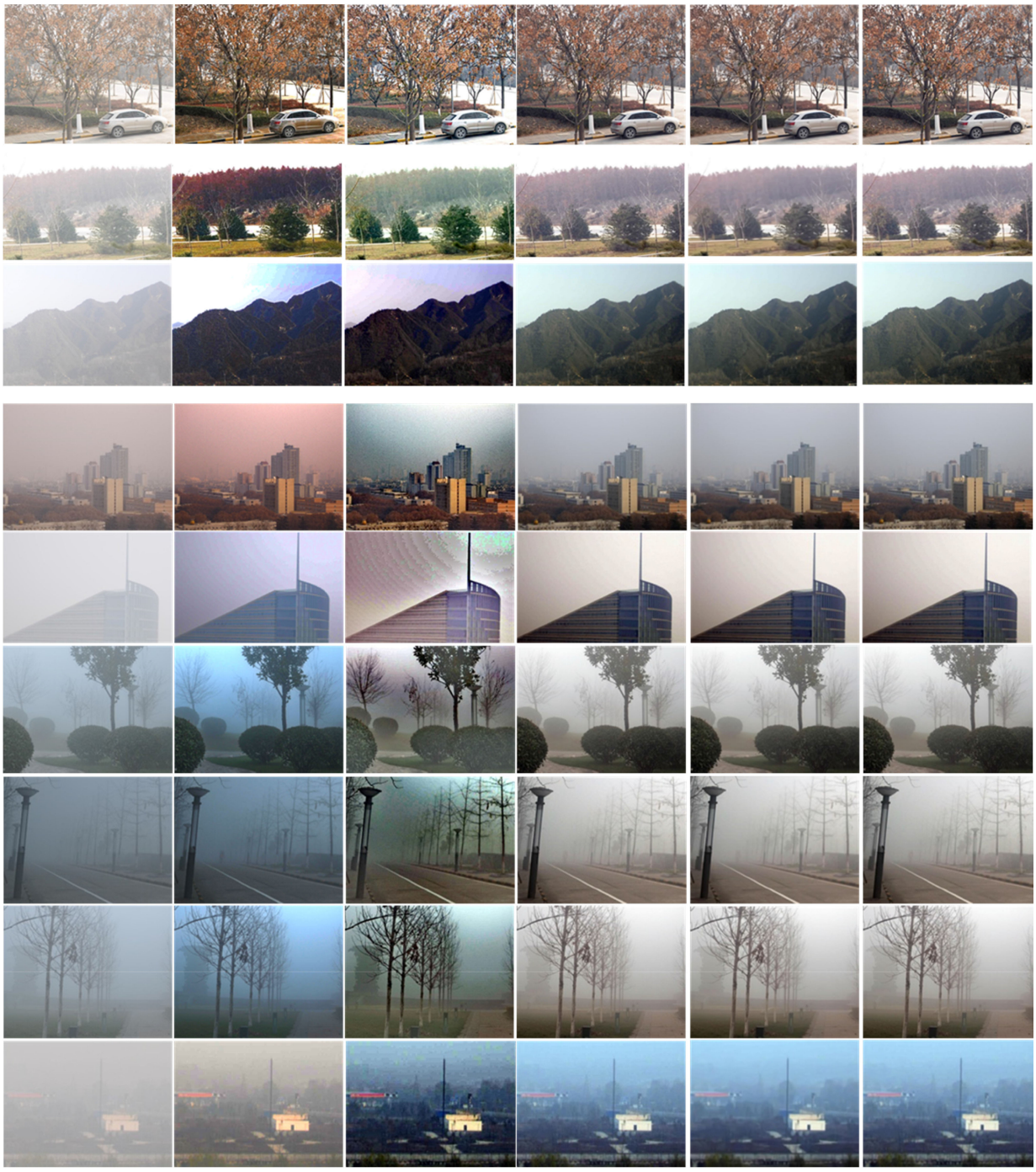

(a) Original scene (b) Dark Channel (c) Non-local (d) Polarization (e) Polarization+BM3D (f) Proposed

Fig. 20. Dehazing results for different images in different days.

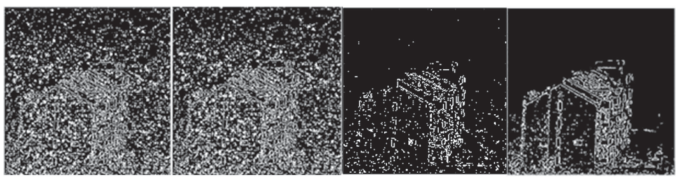

(a) Polarization (b) Dark channel (c) Non-local (d) Proposed

Fig. 21. Visible edges of original image and results of different dehazing methods.

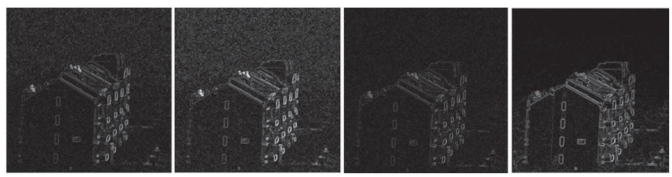

(a) Polarization (b) Dark channel (c) Non-local (d) Proposed

Fig. 22. Gradients of original image and results of different dehazing methods.

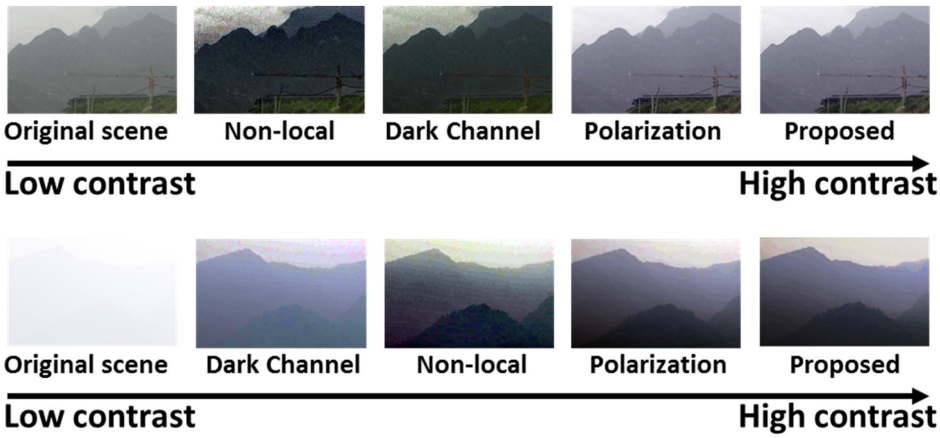

Fig. 23. Evaluation of the final results by CEM.

effect. Comparatively our method gives a better result, and more importantly the sharp edge of the objects is maintained as shown in Fig. 18 and Fig. 19. The BM3D method has resulted in blurry edge and lost the edge information. The experiment results show that the two traditional dehazing method have amplified the noise due to the depth and the high degree of the haze. Even when denoising is applied after dehazing, the noise is sometimes hardly removed and the details can be lost. Many existing dehazing methods fail to take this phenomenon into consideration. For example, a popular dehazing method based on non-local prior concentrates on the similarity of the non-local patches [5]. However, as the patches of similar structure may not have similar level of the noise, applying denosing algorithms invariantly will lead to losses of image details. The proposed dehazing method aims at achieving dehazing and denoising by considering the influence of the transmission map to the noise.

G. Evaluation and Discussions

No-Reference image evaluation is a hard task, especially for polarization images [18], [19], [28]. In [16], authors pointed out that clearer images should have sharper edges and greater gradients, edges or gradients of dehazed images can be used to represent the performance of dehazing. To analyze these results, detected edges are shown in Fig. 21. Although more edges are detected in Figs. 21(a) and (b), the edge images show enormous amount of noise. And Fig. 21(c) shows a loss of edges. It is shown that the proposed method generates the clearest edges and reduces noise. Fig. 21 also demonstrates that existing dehazing methods have amplified the noise level while trying to improve the visibility of a hazy image. In Fig. 22, the images of (a) and (b) has dim gradients of the edges of the scenes and the noise at the background is prominent. The image of (c) shows a loss of details. The gradient images also show that the proposed method performs the best.

A perceptual evaluation using the contrast enhancement metric (CEM) was carried out, and machine learning improve it [28]. A no-reference perceptual fog density prediction model called Fog Aware Density Evaluator (FADE) based on natural scene statistics (NSS) was proposed [17]. Both CEM and FADE correlate well with human judgments. CEM can sort images by their contrast. In FADE, a smaller value means better image quality.

TABLE I
COMPARISON OF THE COMPUTATION TIME FOR THE DIFFERENT METHODS

Method	Dark channel	Non-local	Polarization	Polarization+ BM3D	Proposed
Average Time	3.91s	30.12s	0.12s	44.09s	1.95s

FADE of our results is presented in Table II and in Fig. 3. It correlates well with visual judgments. The FADE evaluation shows that the proposed dehazing method performs better in four of the eight scenarios. For the FADE evaluation uses the nature scene data and it is trained according to a human's intuitive sense, Table II and Fig. 3 could prove our work is mostly outstanding, especially when haze is heavy. Here, we qualitatively compare our method to state-of-the-art dehazing techniques with some real examples.

Fig. 23 presents the CEM of our results. We choose a group of light-hazy results in Fig. 17 and a group of heavy-hazy results in Fig. 18. Then we rank and arrange these results with CEM in order. The CEM is also trained with human's intuitive sense. So the CEM evaluation shows our work performs better in different days.

To show the effectiveness of the proposed iterative scheme, we extract the irradiance of every group of images in the first iteration, which means a one-step optimized operation on the original result with polarization method [10]. We calculate the FADE of these intermediate results which is shown in Table II. We sort the images into two conditions: a light haze condition (the dark channel value less than 150) and a heavy haze condition (the dark channel value higher than 150). From Table II, it can be seen that our method with only one-step iteration performs better than the original polarization method. By analysis the Table II, we can conclude that proposed method obtains the best results in heavy haze than other methods. In light haze condition, part of dehazing results by the proposed method is superior to

TABLE II
EVALUATION RESULTS BY THE METHOD PROPOSED IN [17]

Index	Haze condition	Source figure	Dark channel	Non-local	Polarization	Polarization +BM3D	First iteration	Proposed
FADE	Light Haze (dark channel value less than 150)	Row 1 in Fig.14	0.7958	0.7514	0.8384	0.8417	0.8112	**0.7431**
		Row 2 in Fig.14	0.5896	**0.5445**	0.8577	0.9058	0.7960	0.7577
		Row 3 in Fig.14	2.1063	2.3173	1.8783	1.9270	1.8318	**1.8260**
		Fig.15	0.9641	**0.8655**	1.1063	1.4717	1.0769	0.9925
		Fig.16	**0.7415**	0.8141	1.2458	1.9431	1.1962	1.1870
		Fig.17	**0.8147**	1.3227	0.9058	1.1270	0.9071	0.8922
		Row 1 in Fig.20	0.6324	**0.5336**	0.9706	0.7854	0.8235	0.7003
		Row 2 in Fig.20	0.8147	0.8124	0.9058	0.9270	0.8948	**0.8055**
		Row 3 in Fig.20	0.8854	0.8203	1.1419	0.8218	0.9671	**0.8157**
	Heavy Haze (dark channel value higher than 150)	Row 4 in Fig.14	2.6741	1.9651	1.8685	1.9134	1.8502	**1.6402**
		Fig.18	8.9168	4.5808	4.6614	4.6728	4.5344	**4.3232**
		Fig.19	4.4501	3. 4569	2.7217	3.0978	2.4387	**2.2534**
		Row 4 in Fig.20	2.9872	2.9706	2.1576	2.9649	2.0816	**1.9575**
		Row 5 in Fig.20	3.0975	2.7407	2.9572	2.6787	2.7655	**2.4218**
		Row 6 in Fig.20	3.2785	3.1576	3.1419	2.7577	2.7952	**2.6557**
		Row 7 in Fig.20	3.5469	3.1557	2.9157	2.7431	2.5869	**2.0357**
		Row 8 in Fig.20	4.8147	4.9058	3.6324	3.9134	3.4898	**3.1270**
		Row 9 in Fig.20	7.9575	5.6126	4.7922	4.3922	4.4456	**3.8491**

other methods. And part of dehazing results by dark channel and non-local methods is the best. As in light haze condition, the noise in transmission map and irradiance is very low.

We ran all three algorithms on a computer with Intel R Core E3-1225 3.30 Ghz CPU with 48 GB RAM, and using Matlab R2014b. The images have an average resolution of 708 $\times$ 516 pixels. Table I shows the average computation time per image.

H. The Convergence of Proposed Method

To confirm the convergence of the proposed method, every iteration in dehazing process is tested. Fig. 24 shows the four iterations of transmission of light-hazy image and heavy-hazy image, respectively. Fig. 25 also shows the four iterations of irradiance of light-hazy image and heavy-hazy image.

In our method, we set the step size a small value, $\eta = 0.1$ to ensure the convergence and the convergence can be guaranteed as showed in the figure below where the difference between iteration continues to fall.

To show the convergence of the proposed scheme, we calculate the mean difference of every neighboring iterative images. The specific method is calculating the difference of pixels of the same coordinates of every neighboring iterative images, then calculate the average of the differences. The results of Fig. 25 are shown in Fig. 26. From Fig. 26, it can be seen the mean difference decreases with each iteration. And at the last iteration the mean difference reaches a small value. It shows our iterative method will converge quickly.

A large step size will lead to fast convergence, but could miss the optimal solution. If the step size is too small, the iteration speed is too slow, and the running time is long. And the value of t only ranges from 0 to 1. There is only one condition that the iteration will not converge: the step size is too large.

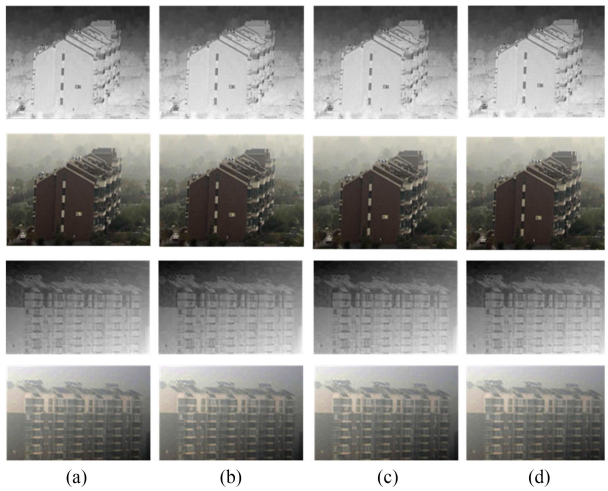

Fig. 24. The row 1 and row 3 demonstrate the four iterative transmission maps of Fig. 16 and Fig. 19. The row 2 and row 4 demonstrate the iterative irradiance maps of Figs. 16 and 19. (a) (b) (c) (d) present the first, second, third and fourth iterative transmission in order.

So, in conclusion, our iteration will converge in general. If not, the problem can be solved by reducing the step size.

I. The Iteration of Dehazing Method

To compare the proposed iterative dehazing method with other non-iterative method fairly, we also iterate the other

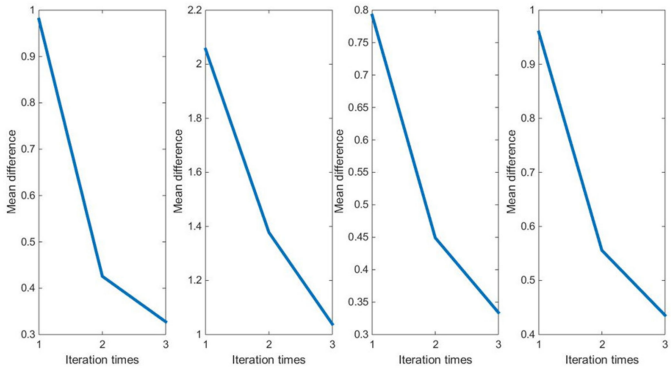

Fig. 25. The mean difference of every neighboring images of Fig. 24.

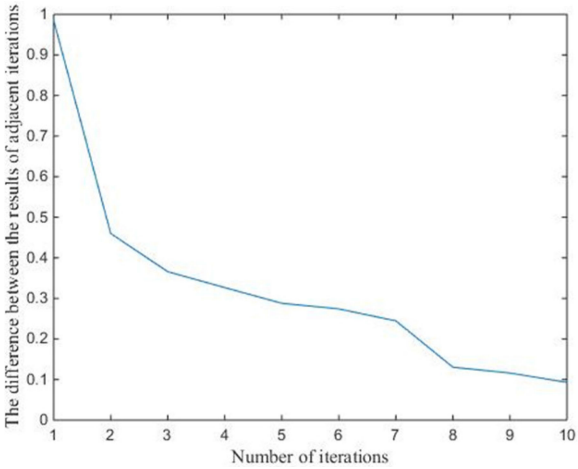

Fig. 26. The mean difference of every neighboring images of Fig. 25(a) in continuing iterations.

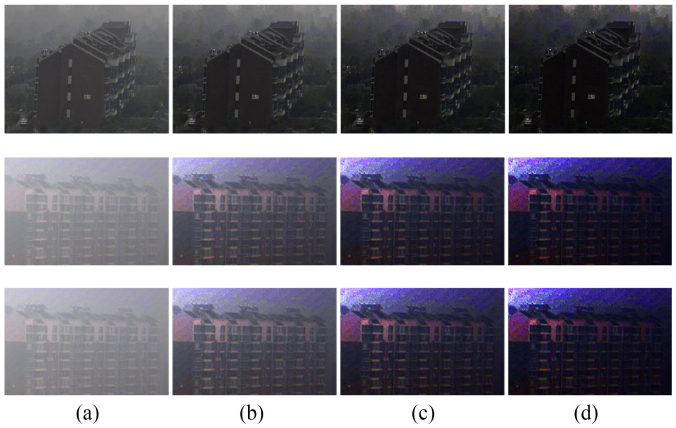

Fig. 27. Iterative irradiance maps of Figs. 16 and 19 with Dark Channel.

methods. The iteration results of other results are shown in Fig. 27. Since the input of Schechner's method is at least two images and output is one image, however, iterative execution is not possible.

Fig. 27 shows that in every iteration, the estimated airlight becomes smaller and transmission map becomes larger compared with the normal value. The result of every iteration becomes darker compared to the result of last iteration. Fig. 28 shows that in every iteration, the estimated airlight becomes larger and transmission map becomes smaller compared to the normal value. The contrast becomes larger, but the distortion becomes heavy in every iteration. Iterative execution of Dark Channel and Non-local methods fail to enhance the original images. In every iteration, the quality of image dehazing of Dark Channel and Non-local declines.

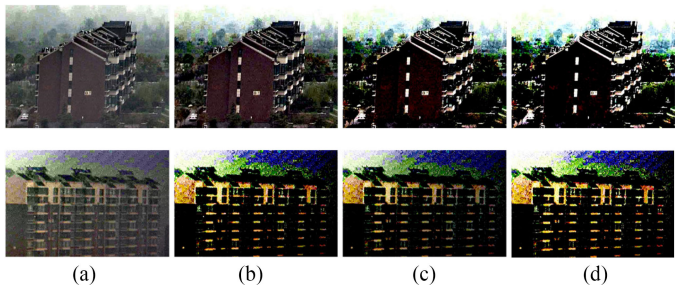

Fig. 28. Iterative irradiance maps of Figs. 16 and 19 with Non-local method.

V. Conclusion

This paper proposes a haze model considering the noise amplification effect in the dehazing process. The method is based on the relation between the level of the noise after dehazing and the scene distance as well as the concentration of the haze. We have proposed an Iterative Dehazing Optimizing Process, an iterative scheme, to suppress the noise produced during the dehazing process incorporating two weighted regularization processes. The experiments show that our method does not only work well with different hazy levels, even in the extreme intensities, it suppresses noise and maintains details.

References

[1] R. T. Tan, "Visibility in bad weather from a single image," in *Proc. IEEE Conf. Comput. Vis. Pattern Recognit.*, 2008, pp. 1–8.
[2] R. Fattal, "Single image dehazing," *ACM Trans. Graph.*, vol. 27, pp. 1–9, 2008.
[3] K. He, J. Sun, and X. Tang, "Single image haze removal using dark channel prior," in *Proc. IEEE Conf. Comput. Vis. Pattern Recognit.*, 2009, pp. 1956–1963.
[4] Y. Bahat and M. Irani, "Blind dehazing using internal patch recurrence," in *Proc. Eur. Conf. Comput. Vis.*, 2014, pp. 783–798.
[5] D. Berman, T. Treibitz, and S. Avidan, "Non-local image dehazing," in *Proc. Comput. Vis. Pattern Recognit.*, 2016, pp. 1674–1682.
[6] K. Tang, J. Yang, and J. Wang, "Investigating haze-relevant features in a learning framework for image dehazing," in *Proc. IEEE Conf. Comput. Vis. Pattern Recognit.*, 2014, pp. 2995–3002.
[7] B. Cai *et al.*, "DehazeNet: An end-to-end system for single image haze removal,"*IEEE Trans. Image Process.*, vol. 25, no. 11, pp. 5187–5198, Nov. 2016.
[8] J. Kopf *et al.*, "Deep photo: Model-based photograph enhancement and viewing," *ACM Trans. Graph.*, vol. 27, pp. 32–39, 2008.
[9] L. Schaul, C. Fredembach, and S. Susstrunk, "Color image dehazing using the near-infrared," in *Proc. IEEE Int. Conf. Image Process.*, 2009, pp. 1629–1632.
[10] Y. Y. Schechner, S. G. Narasimhan, and S. K. Nayar, "Instant dehazing of images using polarization," in *Proc. IEEE Comput. Soc. Conf. Comput. Vis. Pattern Recognit.*, 2001, pp. 325–332.
[11] S. Shwartz, E. Namer, and Y. Y. Schechner, "Blind haze separation," in *Proc. IEEE Comput. Soc. Conf. Comput. Vis. Pattern Recognit.*, 2006, pp. 1984–1991.

[12] D. Miyazaki *et al.*, "Polarization-based dehazing using two reference objects," in *Proc. IEEE Int. Conf. Comput. Vis. Workshops*, 2013, pp. 852–859.
[13] J. Liang *et al.*, "Polarimetric dehazing method for dense haze removal based on distribution analysis of angle of polarization," *Opt. Express*, vol. 23, no. 20, pp. 26146–26157, 2015.
[14] Y. Qu and Z. Zou, "Non-sky polarization-based dehazing algorithm for non-specular objects using polarization difference and global scene feature," *Opt. Express*, vol. 25, no. 21, pp. 25004–25022, 2017.
[15] K. Dabov, A. Foi, and K. Egiazarian, "Video denoising by sparse 3D transform-domain collaborative filtering," in *Proc. Signal Process. Conf.*, 2007, pp. 2080–2095.
[16] N. Hautière, J. P. Tarel, D. Aubert, and É. DUMONT, "Blind contrast enhancement assessment by gradient ratioing at visible edges," *Image Analysis Stereol.*, vol. 27, pp. 87–95, 2008.
[17] L. K. Choi, J. You, and A. C. Bovik, "Referenceless prediction of perceptual fog density and perceptual image defogging," *IEEE Trans. Image Process*, vol. 24, no. 11, pp. 3888–3901, Nov. 2015.
[18] Y. Zhao *et al.*, *Multi-Band Polarization Imaging and Applications*. Berlin, Germany: Springer, 2016.
[19] J. Yang, Y. Zhao, C. Yi, and J. C.-W. Chan, "No-reference hyperspectral image quality assessment via quality-sensitive features learning," *Remote Sens.*, vol. 9, no. 4, pp. 305–328, 2017.
[20] S. Lee *et al.*, "A review on dark channel prior based image dehazing algorithms," *Eurasip J. Image Video Process.*, vol. 2016, no. 1, pp. 4–26, 2016.
[21] C. O. Ancuti and C. Ancuti, "Single image dehazing by multi-scale fusion," *IEEE Trans. Image Process.*, vol. 22, no. 8, pp. 3271–3282, Aug. 2013.
[22] W. Bo, T. Lu, and Z. Xiong, "Adaptive boosting for image denoising: Beyond low-rank representation and sparse coding," in *Proc. IEEE Int. Conf. Pattern Recognit.*, 2017, pp. 1400–1405.
[23] J. Wang, W. Wang, R. Wang, and W. Gao, "CSPS: An adaptive pooling method for image classification," *IEEE Trans. Multimedia*, vol. 18, no. 6, pp. 1000–1010, Jun. 2016.
[24] J. Xie, R. S. Feris, S. S. Yu, and M. T. Sun, "Joint super resolution and denoising from a single depth image," *IEEE Trans. Multimedia*, vol. 17, no. 9, pp. 1525–1537, Sep. 2015.
[25] W. Wang *et al.*, "Fast image dehazing method based on linear transformation," *IEEE Trans. Multimedia*, vol. 19, no. 6, pp. 1142–1155, Jun. 2017.
[26] Y. Song *et al.*, "Single image dehazing using ranking convolutional neural network," *IEEE Trans. Multimedia*, vol. 20, no. 6, pp. 1548–1560, Jun. 2018.
[27] W. Ren, S. Liu, H. Zhang, J. Pan, X. Cao, and M. H. Yang, "Single image dehazing via multi-scale convolutional neural networks," in *Proc. Eur. Conf. Comput. Vis.*, 2016, pp. 154–169.
[28] K. B. Gibson and T. Q. Nguyen, "A no-reference perceptual based contrast enhancement metric for ocean scenes in fog," *IEEE Trans. Image Process.*, vol. 22, no. 10, pp. 3982–3993, Oct. 2013.
[29] X. Fan, Y. Wang, X. Tang, R. Gao, and Z. Luo, "Two-layer Gaussian process regression with example selection for image dehazing," *IEEE Trans. Circuits Syst. Video Technol.*, vol. 27, no. 12, pp. 2505–2517, Dec. 2017.
[30] H. Zhu, X. Peng, V. Chandrasekhar, L. Li, and J.-H. Lim, "Dehazegan:When image dehazing meets differential programming," in *Proc. 27th Int. Joint Conf. Artif. Intell.*, Jun. 2018, pp. 1234–1240.
[31] B. Li *et al.*, "AOD-Net: All-in-one dehazing network," in *Proc. IEEE Int. Conf. Comput. Vis.*, 2017, pp. 4780–4788.

Authors' photographs and biographies not available at the time of publication.